Atmos. Meas. Tech. Discuss., 7, 4659–4692, 2014
www.atmos-meas-tech-discuss.net/7/4659/2014/
doi:10.5194/amtd-7-4659-2014
© Author(s) 2014. CC Attribution 3.0 License.

Atmospheric Measurement Techniques
Discussions
Open Access

This discussion paper is/has been under review for the journal Atmospheric Measurement Techniques (AMT). Please refer to the corresponding final paper in AMT if available.

Long-term evolution and seasonal modulation of methanol above Jungfraujoch (46.5° N, 8.0° E): optimisation of the retrieval strategy, comparison with model simulations and independent observations

W. Bader[1], T. Stavrakou[2], J.-F. Muller[2], S. Reimann[3], C. D. Boone[4], J. J. Harrison[5], O. Flock[1], B. Bovy[1], B. Franco[1], B. Lejeune[1], C. Servais[1], and E. Mahieu[1]

[1]Institute of Astrophysics and Geophysics of the University of Liège, Liège, Belgium
[2]Belgian Institute for Space Aeronomy, Avenue Circulaire 3, 1180, Brussels, Belgium
[3]Laboratory for Air Pollution and Environmental Technology, Swiss Federal Laboratories for Materials Testing and Research (Empa), Duebendorf, Switzerland
[4]Department of Chemistry, University of Waterloo, Ontario, Canada
[5]Department of Chemistry, University of York, York, UK

Received: 11 April 2014 – Accepted: 24 April 2014 – Published: 8 May 2014

Correspondence to: W. Bader (w.bader@ulg.ac.be)

Published by Copernicus Publications on behalf of the European Geosciences Union.

CC BY

Abstract

Methanol (CH_3OH) is the second most abundant organic compound in the Earth's atmosphere after methane. In this work, we present the first long-term time series of methanol total, lower tropospheric and upper tropospheric-lower stratospheric partial columns derived from the analysis of high resolution Fourier transform infrared solar spectra recorded at the Jungfraujoch station (46.5° N, 3580 m a.s.l.). The retrieval of methanol is very challenging due to strong absorptions of ozone in the region of the selected υ_8 band of CH_3OH. Two wide spectral intervals have been defined and adjusted in order to maximize the information content. Methanol does not exhibit a significant trend over the 1995–2012 time period, but a strong seasonal modulation characterized by maximum values and variability in June–July, minimum columns in winter and a peak-to-peak amplitude of 130 %. In situ measurements performed at the Jungfraujoch and ACE-FTS occultations give similar results for the methanol seasonal variation. The total and lower tropospheric columns are also compared with IMAGESv2 model simulations. There is no systematic bias between the observations and IMAGESv2 but the model underestimates the peak-to-peak amplitude of the seasonal modulations.

1 Introduction

Methanol (CH_3OH) is the second most abundant organic molecule in the atmosphere after methane with concentrations between 1 (Singh et al., 2001) and 20 ppbv (Heikes et al., 2002), despite a lifetime that has been estimated to lie between 4.7 days (Millet et al., 2008) and 12 days (Atkinson et al., 2006). Plant growth is the largest source of methanol with a 65–80 % contribution to its emissions (Galbally and Kirstine, 2002; Jacob et al., 2005). The atmospheric production of CH_3OH through peroxy radical reactions represents up to 15–23 % of its sources (Madronich and Calvert, 1990; Tyndall et al., 2001). Other sources of methanol are plant matter decaying (Warneke, 1999),

AMTD
7, 4659–4692, 2014

CC BY

biomass burning (Dufour et al., 2006; Paton-Walsh et al., 2008), fossil fuel combustion, vehicular emissions, solvents and industrial activities.

Methanol influences the oxidizing capacity of the atmosphere through reaction with the hydroxyl radical (Jimenez et al., 2003), its main sink, leading to the formation of water vapour and either CH_3O or CH_2OH radicals which both react with O_2 to give HO_2 and formaldehyde (H_2CO) (Millet et al., 2006). The photo-oxidation of formaldehyde, a key intermediate in the oxidation of numerous volatile organic compounds, leads to the formation of HO_2 radicals and carbon monoxide (CO). As a consequence, CH_3OH is considered as a source of CO with a yield close to 1 (Duncan et al., 2007). The main sources and sink of methanol are characterized by significant seasonal modulations. This results in a strong signal for CH_3OH, with maximum and minimum abundances observed in the Northern Hemisphere at the beginning of July and in December, respectively (Rinsland et al., 2009; Stavrakou et al., 2011; Wells et al., 2012; Cady-Pereira et al., 2012), reflecting the seasonality of biogenic sources.

In the last decade, ground-based (Schade and Goldstein, 2001, 2006; Karl et al., 2003; Carpenter et al., 2004), ship (Warneke et al., 2004) and aircraft (Singh et al., 2006; Fehsenfeld et al., 2006) in situ measurements combined to space-based detections including the Infrared Atmospheric Sounding Interferometer (IASI) onboard the MetOp-A satellite (Razavi et al., 2011), the TES (Tropospheric Emission Spectrometer) nadir-viewing Fourier transform spectrometer (FTS), on board the Aura satellite (Beer et al., 2008), and the solar occultations recorded by the Atmospheric Chemistry Experiment-FTS (ACE-FTS, Bernath et al., 2005; Dufour et al., 2006, 2007) have supplied numerous observations of CH_3OH which have provided valuable insights on the distribution and budget of methanol at the global scale. However, there still remain large uncertainties in our knowledge of the methanol global sources and sinks in the atmosphere, as indicated by the large discrepancies existing between different measurement-based estimates of the total sources (Galbally and Kirstine, 2002; Tie et al., 2003; von Kuhlmann et al., 2003a, b; Jacob et al., 2005; Millet et al., 2008; Stavrakou et al., 2011). Previous studies have reported the measurement of

AMTD
7, 4659–4692, 2014

CC BY

methanol from ground-based infrared solar absorption observations performed at Kitt Peak (31.9° N, 111.6° W, 2090 m a.s.l.; Rinsland et al., 2009) and at Saint-Denis (Reunion Island, 21° S, 55° E, 50 m a.s.l.; Stavrakou et al., 2011; Vigouroux et al., 2012).

In this paper, we report the first methanol time series derived from ground-based high-resolution infrared spectra recorded with a Fourier Transform InfraRed (FTIR) spectrometer operated under clear sky conditions at the high-altitude International Scientific Station of the Jungfraujoch (ISSJ, Swiss Alps, 46.5° N, 8.0° E, 3580 m a.s.l.; Zander et al., 2008). Most of the available spectra have been recorded within the framework of the Network for Detection of Atmospheric Composition Change monitoring activities (NDACC; see http://www.ndacc.org). A detailed analysis was conducted to optimize the retrieval strategy of atmospheric methanol in order to minimize the fitting residuals while maximizing the information content. A thorough discussion of the retrieval strategy, data characterization (information content and error budget), long-term trend and seasonal cycle of total and partial columns of methanol above Jungfraujoch is presented here. This paper is organized as follows. A detailed description of the optimized retrieval strategy is given in Sect. 2. The characterisation of our data by their eigenvectors and error budget is discussed in Sect. 3. Finally, in Sect. 4, we present and discuss the results, focusing on the intra-annual and intra-day variability of methanol at ISSJ along with comparisons with in situ measurements, satellite occultations and model calculations.

2 Retrieval strategy

Regular FTIR observations have been carried out at the ISSJ with a homemade spectrometer since 1984, complemented in the early 1990s and definitely replaced in 2000 by a commercial Bruker IFS120HR instrument (Zander et al., 2008). This spectrometer is equipped with HgCdTe and InSb cooled detectors, allowing us to cover the 650 to 4500 cm^{-1} region of the electromagnetic spectrum. Since 1991, the FTIR instruments are affiliated to the NDACC network.

AMTD
7, 4659–4692, 2014

The Bruker observational database consists of more than 6500 spectra recorded between 1995 and 2012 with an optical filter covering the 700 to 1400 cm^{-1} domain encompassing the fundamental C-O stretching mode υ_8 of methanol at 1033 cm^{-1}. Spectral resolutions, defined as the reciprocal of twice the maximum optical path difference, alternate between 0.004 and 0.006 cm^{-1}. Signal-to-noise (S/N) ratios vary between 250 and 1800 (average spectra resulting from several successive individual Bruker scans, when solar zenith angles vary slowly). The optimization of the retrieval strategy was based on a subset of 314 spectra covering the year 2010.

The CH_3OH column retrievals and profile inversions have been performed using the SFIT-2 v3.91 fitting algorithm. This retrieval code has been specifically developed to derive mixing ratio profiles of atmospheric species from ground-based FTIR spectra (Rinsland et al., 1998). It is based on the semi-empirical implementation of the Optimal Estimation Method (OEM) developed by Rodgers (1990). Vertical profiles are derived from simultaneous fits to one or more spectral intervals in at least one solar spectrum with a multilayer, line-by-line calculation that assumes a Voigt line shape (Drayson, 1976). The model atmosphere adopted above the Jungfraujoch altitude consists in a 39 layers scheme with progressively increasing thicknesses, from 3.58 km to reach the 100 km top altitude. The pressure-temperature profiles are provided by the National Center for Environmental Prediction (NCEP, Washington DC, USA, http://www.ncep.noaa.gov/) while the solar line compilation supplied by F. Hase (KIT) (Hase et al., 2006) has been assumed for the solar absorptions. Line parameters used in the spectral fitting process were taken from the HITRAN 2008 spectroscopic compilation (Rothman et al., 2009). Methanol lines have been added to the HITRAN compilation for the first time in 2004 (Rothman et al., 2005). The parameters for the 10 µm region are described in the paper by Xu et al. (2004) and were derived from measurements with two high-spectral resolution FTS instruments.

Two spectral windows both encompassing the υ_8 C-O stretch absorption band of methanol have been defined. Synthetic spectra (6.1 mK, zenith angle of 80°) have been computed for the first and second order absorbers in both selected windows

AMTD
7, 4659–4692, 2014

and are illustrated on Fig. 1. The first interval ranges from 992 to 1008.3 cm^{-1} and is based on windows used in previous investigations. A 992–998.7 cm^{-1} window was employed for the retrieval of CH_3OH from Kitt Peak FTS spectra (Rinsland et al., 2009) and a 984.9–998.7 cm^{-1} window was used for the initial retrievals of methanol from ACE-FTS occultation observations (Dufour et al., 2007). The latest ACE-FTS CH_3OH retrievals (version 3.5) use an extended window from 984.9 to 1005.1 cm^{-1}. Measuring in the limb, ACE-FTS measurements start to saturate for wavenumbers above 1005.1 cm^{-1} for occultations with higher than average O_3 levels. As ground based observations do not have this problem, we included supplemental methanol features up to the 1008.3 cm^{-1} limit. The second interval, ranging from 1029 to 1037 cm^{-1} is used by Vigouroux et al. (2012).

Absorption by the main ozone isotopologue (^{16}O-^{16}O-^{16}O or O_3) captures nearly 93 % and 98 % of the IR radiation in the "1008" and "1037" windows respectively and is close to saturation in the latter one. Methanol features are much weaker with respectively mean absorption of 1.7 and 1.8 % for the "1008" and the "1037" windows. Additional absorptions are associated to O_3 isotopologues, such as O_3(668) or (^{16}O-^{16}O-^{18}O), O_3(686) or (^{16}O-^{18}O-^{16}O), O_3(676) or (^{16}O-^{17}O-^{16}O) and O_3(667) or (^{16}O-^{16}O-^{17}O) as well as carbon dioxide (CO_2) and water vapour (H_2O). Since the CH_3OH absorption lines are quite weak, only spectra with solar zenith angles greater than 65° and up to 80° have been analyzed. During the retrievals, both windows were for the first time fitted simultaneously.

The a priori mixing ratio profile for the CH_3OH target is a zonal mean (for the 41–51° N latitude band) of 903 occultations recorded by the ACE-FTS instrument (version 3.5) between the 27 March in 2004 and the 3 August in 2012 extending from 5.5 to 30 km tangent altitudes. The profile was extrapolated to 1 ppbv to the surface (Singh et al., 2001; Heikes et al., 2002), and to 0.05 ppbv (Singh et al., 2006; Dufour et al., 2007) for upper layers. The covariance matrix is specified for each layer as a percentage of the a priori profile and an ad hoc correlation length, which is interpreted as a correlation between layers decaying along a Gaussian. For methanol, we adopted

AMTD
7, 4659–4692, 2014

CC BY

a 50 % km^{-1} diagonal covariance and a Gaussian half width of 4 km for extra diagonal elements. A priori profiles for all interfering molecules are based on the WACCM (version 5, the Whole Atmosphere Community Climate Model, e.g. Chang et al., 2008) model climatology for the 1980–2020 period and the ISSJ station. The vertical profiles of CH_3OH, O_3 and O_3(668) are fitted during the iterative process while the a priori distributions of O_3(686), O_3(676), O_3(667), H_2O and CO_2 are scaled. Since the fitting quality is significantly different in both windows, two different values for the signal-to-noise for inversion have been selected, i.e. 180 and 40 for the "1008" and "1037" domains, respectively.

When fitted independently, we observe a compact correlation between the corresponding CH_3OH total columns retrieved from both windows with a small bias of 15 ± 13 % (2-σ). When comparing ozone total columns respectively retrieved from the strategy described in this work and from the retrieval strategy applied within the NDACC network (window limits: 1000–1005 cm^{-1}, Vigouroux et al., 2008), no significant bias emerges from the comparison between the two ozone total columns sets, with a mean relative difference of −0.8 ± 2.4 % (2-σ), demonstrating a proper fit of the main interference involved in our methanol retrieval strategy. Additional functions are also included in the fitting process to account for deviations from a perfectly aligned FTS. As an effective apodization function, we assumed a polynomial function of order 2 (Barret et al., 2002). The effective apodization parameter (EAP) gives the value of the effective apodization function at the maximum optical path difference and is synonymous of a well-aligned instrument when it is close to 1.0. The inversion of the EAP has been included in our retrieval as well as in the NDACC's retrieval strategy of ozone. The EAP derived from both strategies proved to be consistent, with a mean relative difference of 0.7 ± 2.6 % (2-σ). Those three latter points give confidence in the combination of the two selected windows and in our optimized retrieval strategy.

AMTD
7, 4659–4692, 2014

cc BY

3 Data characterization and error budget

Information content has been carefully evaluated and typical results are displayed on Fig. 2. The information content is significantly improved, with a typical Degree Of Freedom for Signal (DOFS) of 1.82, in comparison with DOFS of about 1 in previous studies (e.g., Rinsland et al., 2009; Vigouroux et al., 2012). In Fig. 2, the first eigenvector and eigenvalue (see left panel, in orange) show that the corresponding information is mainly coming from the retrieval (99 %). The increase of information content allows us to retrieve a tropospheric column (Tropo, from 3.58 to 10.72 km) with only 1 % of a priori dependence as well as two partial columns with less than 30 % of a priori dependence (second eigenvector) i.e. a low-tropospheric (LT, from 3.58 to 7.18 km) and an upper troposphere-lower stratosphere (UTLS, from 7.18 to 14.84 km).

The error budget is calculated following the formalism of Rodgers (2000), and can be divided into three different error sources: the smoothing error expressing the uncertainty due to finite vertical resolution of the remote sounding system, the forward model parameters error, and the measurement noise error. The right panel of Fig. 2 gives the corresponding error budget, with identification of the main error components, together with the assumed variability. Error contributions for total and all three partial columns are reported in Table 1.

Through a perturbation method, we also accounted for other error sources: systematic errors such as the spectroscopic line parameters and the misalignment of the instrument while uncertainty on the temperature and on the solar tracking is considered to be source of random error. Table 1 provides an error budget resulting from major instrumental and analytical uncertainties. For the spectroscopic line parameters, we included in our error budget the uncertainty on line intensities provided by the HITRAN database. As methanol line intensities matter, a rough idea of the accuracy of the intensities can be obtained from Table 8 of Xu et al. (2004) work as it reports an RMS deviation of 7 %. It should be noted that the uncertainty on ozone and its isotopologues lines, according to HITRAN-08 parameters, amounts to between 5 and 10 % (Rothman

AMTD
7, 4659–4692, 2014

et al., 2009). However, an extremely high accuracy of ozone spectroscopic parameters is required in order to retrieve methanol columns properly. We noted that the SFIT-2 algorithm fails to perform a satisfying retrieval when using spectroscopic parameters with ozone lines incremented by 10 %, suggesting that the error on the concerned lines is more likely to be closer to 5 (or even lower) than to 10 %. Therefore, we accounted for an error on ozone and its isotopologues line intensities of 5 % in our error budget.

We accounted for an error of 10 % on the instrument alignment at the maximum path difference. By comparing the two official NDACC algorithms, Hase et al. (2004) and Duchatelet et al. (2010) have established that the forward model may induce a maximum error of one percent on the retrieved columns for a suite of FTIR target gases. The uncertainty on the pressure-temperature profiles is provided by NCEP with an error of 1.5 K from the ground to an altitude of about 20 km. Concerning the upper levels the uncertainty increases with altitude, from 2 K around 25 km until 9 K at the top. The uncertainty on the solar zenith angle (SZA) is estimated at 0.2°.

We also provide in Table 1 the mean relative standard deviation for each daily mean for days with 3 or more measurements. It is found to be of the same order of magnitude than the random error. The dominant contribution to the systematic error is the error on methanol spectroscopic lines, while the measurement noise error is the main component of random error. Both systematic and random errors are given in Table 1, with 7 % and around 5 % respectively on the total columns.

4 Results and comparisons

Since the improvement in information content allows us to compute partial columns with only a 30 % a priori dependence and as the random error on the tropospheric column is about 4 times the error on total columns (see Table 1), we focus our trend analysis on total, LT and UTLS columns. Therefore, an analysis of the seasonal variation of methanol in the lower-troposphere and the UTLS has been performed, including comparisons with in situ measurements (Legreid et al., 2008) and to ACE-FTS occultation

CC BY

observations, respectively. Comparisons with simulations obtained from the IMAGESv2 global chemistry-transport model (Stavrakou et al., 2011) have also been conducted.

4.1 Data description

In situ measurements have been performed at the ISSJ station from air samples collected on a two-stage adsorbent system connected to a gas chromatograph–mass spectrometer (GC-MS; Legreid et al., 2008). The system was in operation during four measurement campaigns in 2005 which were performed from 8 February until 8 March 2005 for the winter measurements, spring measurements followed from 22 April until 30 May, in summertime measurements start from 5 August until 19 September and fall measurements from 14 October until 1 November with a frequency of about one sample every 50 min. A total of 1848 measurements of methanol on 122 days have been compared with our lower-tropospheric column time series for the year 2005.

Monthly mean UTLS columns have been derived from measurements taken by the ACE-FTS instrument and compared to our UTLS product. We selected and converted into partial columns the mixing ratios measured by ACE-FTS during ∼ 140 occultations performed in the altitude range of 7.5–14.5 km (version 3.5; Boone et al., 2013) in the 41.5 to 51.5 northern latitude zone between the 30 March 2004 and the 20 February 2013.

Two model simulations of daily methanol mixing ratios in the 2004–2012 time period obtained from the IMAGESv2 global chemistry-transport model (fully described in Stavrakou et al., 2011) are presented here. The IMAGESv2 model was run at a resolution of 2° in latitude and 2.5° in longitude and with a time step of 6 h. It has 40 vertical (hybrid sigma-pressure) levels between the Earth's surface and the lower stratosphere (44 hPa). Daily averaged mixing ratios calculated by the model at the model pixel comprising the ISSJ station were used to calculate the partial and total columns above the station. The first simulation "MEGAN", is performed using MEGANv2.1 bottom-up emissions which are calculated using an emission model fitted to net ecosystem flux

AMTD
7, 4659–4692, 2014

CC BY

measurements. The second one, "IASI", uses emissions constrained by IASI vertical column data in an inverse modelling framework based on the adjoint of IMAGESv2.

4.2 Time series and long term trend

In order to produce the first long-term time series of atmospheric methanol above Jungfraujoch, three criteria were used to reject noisy measurements or weak absorption: (i) when negative methanol mixing ratios are retrieved, (ii) when rms (root mean square, difference between calculated and observed absorption) was out of the interval defined by the 95 % level of confidence (2-σ), (iii) when the number of iterations reached the fixed maximum. After implementation of these criteria, the total number of valid measurements is 4271 obtained on 1476 days of measurements between 1995 and 2012. For the trend calculations, we used the statistical tool developed by Gardiner et al. (2008) that employs a bootstrap resampling method. The function fitted to the time series is a combination of a linear component and a 3rd order Fourier series, i.e.:

$$F(t,b) = c0 + c(t-t0) + b1\cos 2\pi(t-t0) + b2\sin 2\pi(t-t0) + b3\cos 4\pi(t-t0) \\ + b4\sin 4\pi(t-t0) + b5\cos 6\pi(t-t0) + b6\sin 6\pi(t-t0) \quad (1)$$

where c_0 is the abundance at the reference time t_0 for the linear component (seasonalized data), and c is the annual trend. Figure 3 shows the whole times series of daily mean methanol total columns above Junfraujoch. We evaluated the trend of methanol total columns over the 1995–2012 time period and found a yearly negative trend of $(-1.34 \pm 2.71) \times 10^{13}$ molecules cm^{-2} or -0.18 ± 0.36 % (2-σ), i.e. a non-significant trend at this level of confidence which is consistent with the trend computed by Rinsland et al. (2009). A non-significant trend has been computed also for both partial column subsets. Hence the results indicate a long-term trend which is not statistically significant and a strong seasonal variation.

AMTD
7, 4659–4692, 2014

CC BY

4.3 Methanol seasonal modulation

As the results for the full time series do no indicate a statistically significant trend, we illustrate in Fig. 4 the daily mean total columns over a 1 year time base. The strong seasonal modulation of methanol is characterized by minimum values and variability in December to February and maximum columns in June–July. The methanol maximum in summer indicated by our results is consistent with the maximum observed for free tropospheric methanol above Kitt Peak (Rinsland et al., 2009) and the analysis of IASI tropospheric measurements over Europe (Razavi et al., 2011). The mean peak-to-peak amplitude of a seasonal cycle computed by Gardiner's tool and expressed as a percentage of the corresponding CH_3OH yearly mean column amounts to 130.1 ± 1.6 % (2-σ) while the seasonal modulation above Kitt Peak amounts to 64.6 ± 0.1 % showing a similar amplitude with the IASI measurements (Razavi et al., 2011) for subtropical regions.

The IMAGESv2 model estimates a seasonal modulation of methanol in phase with the one we measured but underestimate the peak-to-peak amplitude with 88.6 ± 1.3 % and 70.4 ± 1.2 % for "IASI" and "MEGAN" respectively. The MEGAN emission fluxes being dependent on temperature, visible ration fluxes, leaf area index and leaf age, they show a pronounced seasonal variation at mid-latitudes, with peak values in early summer. The IASI-derived emissions peak somewhat earlier than in the MEGAN inventory, a result consistent with modeling studies using TES methanol data (Wells et al., 2012; Cady-Pereira et al., 2012) as well as with other studies based on in situ concentration measurements (Jacob et al., 2005) or on flux measurements (Laffineur et al., 2012) which concluded to substantially higher methanol emission rates by young leaves compared to mature or senescent leaves.

No systematic bias is observed on the whole time series, but a seasonal bias is characterized (see Fig. 4): the maximum fractional difference [(IMAGES-FTIR)/((IMAGES+FTIR)/2)] between monthly mean results from FTIR measurements and both "IASI" and "MEGAN" simulations is found to occur in July, with

AMTD
7, 4659–4692, 2014

−45 ± 27 % and −39 ± 28 %, respectively. The minimum fractional difference amounts to 28 ± 20 % and 38 ± 19 % respectively in January and shows an overestimation of methanol during wintertime by the IMAGESv2 model. The underestimation of methanol by the "IASI" simulation during summertime is unexpected, since this simulation reproduced very well the methanol total columns measured by IASI over Western Europe (Fig. 5 in Stavrakou et al., 2011). Noting that ISSJ does not sample the lower troposphere below 3.58 km altitude, this discrepancy might reflect an overestimation of the simulated vertical gradient of methanol mixing ratios at continental mid-latitudes, which is suggested by comparisons with aircraft campaigns in spring and summer over the United States (Stavrakou et al., 2011). It is not clear, however, why this issue does not lead also to a similar model underestimation of the methanol column above ISSJ in spring. The overestimated gradient in IMAGES may be due to a well-known problem in chemical transport models, i.e. the overestimation of the hydroxyl radical concentration in the Northern Hemisphere (Krol and Lelieveld, 2003). It could also be related to the large uncertainties in the ocean/atmosphere flux of methanol, given that even the sign of this flux is not well constrained (Millet et al., 2008), and since IASI data were not considered as sufficiently reliable over the ocean in the optimization of emissions using IMAGES by Stavrakou et al. (2011).

4.4 Methanol diurnal variation

The variation of the methanol abundance throughout the day has also been characterized on Fig. 5. To this end, we extended the targeted range of solar zenith angle (SZA) going from 30 to 85° and selected only those whose retrieval provided a DOFS of at least 1. Due to the large seasonal variation, we divided our measurements into 3 subsets corresponding to summer (June, July, Augustus), winter (December, January, February) and the rest of the year. Even though we found no significant trend of methanol through the day in summer, a significant increase during winter and the rest of the year has been evaluated at 0.4 ± 0.3 and 1.1 ± 0.2 % $^{\circ}C^{-1}$ respectively in the morning while methanol decreases through the afternoon at a rate of respectively

AMTD
7, 4659–4692, 2014

CC BY

-0.9 ± 0.2 and $-0.5 \pm 0.1\,\%\,^{\circ}C^{-1}$. A rough approximation of those trends gives an increase of approximately 5.5×10^{13} and 2.7×10^{14} molecules $cm^{-2}\,h^{-1}$ in the morning and to a decrease of -1.6×10^{14} and -1.9×10^{14} molecules $cm^{-2}\,h^{-1}$ in the afternoon for winter and the rest of the year, respectively.

The causes for the observed diurnal variation are not clear. Major methanol sources such as biogenic production by living plants and photochemical production are stronger during daytime, due to the key role played by solar radiation in photosynthesis and other biotic processes, as well as in the generation of OH radicals through photolytic processes (Logan et al., 1981). However, these sources are expected to peak during the summer, when the diurnal variation of the column is found to be negligible. Since the photochemical sink of methanol (i.e. reaction with OH) is strongest during the day, the observed diurnal variation (and absence thereof during summer) could result from the variable balance between sources and sinks. However, OH fields, produced by the GEOS-CHEM model (Bey et al., 2001) have been examined and no direct correlation with our methanol total columns has been found. Moreover, since the IMAGES model includes those processes but still fails to reproduce the observed diurnal variation, it appears likely that other factors play a significant role, e.g. orography-induced wind patterns bringing boundary layer air to the free troposphere above the station's altitude. Besides model simulations, in situ measurements have also been explored. However, the existing datasets being "campaign-type", the statistics are too weak to draw clear conclusions on this subject. More efforts should be put in further research on processes governing the methanol diurnal variation.

4.5 Methanol in the lower troposphere

On Fig. 6, our lower tropospheric columns show a seasonal modulation with characteristics close to the seasonal variation of total columns with similar occurrence of maximum and minimum but a wider peak-to-peak amplitude of $168 \pm 3\,\%$. The upper panel of Fig. 6 also shows monthly fractional differences between the FTIR results and

AMTD
7, 4659–4692, 2014

both simulations from the IMAGESv2 model (Stavrakou et al., 2011) as well as seasonal differences with in situ measurements performed at the Jungfraujoch (Legreid et al., 2008).

None of the IMAGESv2 series stands out, since they both underestimate the peak-to-peak amplitude with 78 ± 2 % and 101 ± 2 % for MEGAN and IASI, respectively. For both series, methanol is overestimated in winter (DJF) and shows a good agreement in spring (MAM) as well as in October and November. During summertime, results during July are significantly underestimated but the difference for the remaining 3 months (June, Augustus and September) is close to non-significant.

The seasonal amplitude of the in situ measurements is significantly lower than in the FTIR data, although a good agreement is found on the data dispersion (see error bars) except for the fall season with more compact values. The high standard deviation in summer appears to be due to only a few days with high methanol mixing ratios. These days are characterized by trajectories originating from the South, where biogenic sources are more active. Indeed, it has been established by Legreid et al., 2008, that there is a considerable contribution of methanol from the south which is reasonable since methanol is emitted in large amounts from biogenic sources (Fall, 2003; Jacob et al., 2002, 2005; Singh et al., 1994), which because of the warmer climate are more active in the south of the Alps than in the north. Furthermore, air masses from the South are transported over Northern Italy, which is a highly industrialized area with considerable anthropogenic emissions.

4.6 Methanol in the upper troposphere-lower stratosphere (UTLS)

The comparison between the UTLS FTIR columns, both IMAGES datasets and monthly mean results from ACE-FTS occultations illustrated on Fig. 7 shows an overall good agreement. As for total and lower-tropospheric columns, methanol variability is underestimated by the IMAGESv2 model. On the other hand, the seasonal cycle of methanol UTLS columns is satisfactorily characterized by FTIR results and the IMAGES simulations in terms of absolute value with a non-significant fractional difference with FTIR

CC BY

of −6 ± 49 % and 1 ± 48 %, respectively for MEGAN and IASI. The peak-to-peak amplitudes of the three series, i.e. 93 ± 2 % for FTIR, 82 ± 2 for MEGAN and 92 ± 2 % for IASI are in very good agreement as well as the timing of the maximum (June–July).

A close to statistical agreement is observed between Jungfraujoch results and the UTLS columns derived from ACE-FTS data with a mean fractional difference of 33 ± 30 % despite substantially higher ACE methanol columns in March and May. The differences for these two months may be attributed to the fact that monthly mean results from ACE-FTS encompass a 10° latitudinal band and therefore occultations may be capturing local events such as plumes from biomass burning out of range for the Jungfraujoch station.

Biases in the ACE methanol retrievals have recently been addressed by Harrison et al. (2012). Adoption of a new set of infrared absorption cross sections for methanol led to the determination of ACE UTLS columns higher by up to 25 % (calculations based two occultations; see Fig. 6 of Harrison et al., 2012), depending on the temperature of the measurement. Therefore, by applying those new cross sections to our Jungfraujoch retrievals, we would likely identify a bias in the same range, depending on the season and thus the vertical temperature distribution. The effect on total (and partial) columns will have to be evaluated on the basis of larger statistics, for each season and using the new cross sections of Harrison et al. (2012).

5 Conclusions

A long-term time series of methanol has been determined from the analysis of a 17 year time series of infrared solar absorption spectra recorded with a commercial Fourier transform spectrometer Bruker IFS120HR, operated at the high-altitude International Scientific Station of the Jungfraujoch (ISSJ, Swiss Alps, 45° N, 8.0° E, 3580 m a.s.l.; Zander et al., 2008).

The results were analyzed using the SFIT-2 v3.91 fitting algorithm and thanks to the combination of spectral windows used in previous work for the retrieval of methanol

AMTD
7, 4659–4692, 2014

Title Page
Abstract | Introduction
Conclusions | References
Tables | Figures
◀| |▶
◀ ▶
Back | Close
Full Screen / Esc
Printer-friendly Version
Interactive Discussion

CC BY

from FTS spectra (Dufour et al., 2007; Rinsland et al., 2009; Vigouroux et al., 2012), we have significantly improved the information content. With a typical DOFS of 1.82, a total column and two partial columns time series are available, i.e. a lower-tropospheric (LT, 3.58–7.18 km) and an upper tropospheric-lower stratospheric one (UTLS, 7.18–14.84 km). Both random and systematic error sources have been identified and characterized using the spectra recorded in the year 2010, and are found to be respectively 5 and 7 % for the total column.

The analysis of the time series does not reveal a significant long-term trend but shows a high peak-to-peak amplitude of the seasonal cycle of 129.4 ± 5.5 % (2-σ) for total columns. Methanol total and partial columns are characterized by a strong seasonal modulation with minimum values and variability in December to February and maximum columns in June–July. First analysis of methanol diurnal variation shows an increase of methanol in the morning and a decrease during the afternoon for all seasons but summer.

Comparisons with methanol measurements obtained with other techniques (in situ and satellite) give satisfactory results. Although the seasonal amplitude is larger in the FTIR lower tropospheric data compared to in situ measurements, a good agreement is generally found regarding the data dispersion. Concerning the UTLS partial columns, there is a close to statistical agreement with ACE-FTS occultations despite higher ACE columns of methanol in March and May.

The IMAGESv2 simulations underestimate the peak-to-peak amplitude for total and lower-tropospheric columns. Despite the absence of a systematic bias between our results and the IMAGESv2 simulations, comparisons show seasonal differences with an overestimation of winter methanol and an underestimation during summertime, which might be explained by an overestimation of the vertical gradient of methanol mixing ratios by the model. Regarding UTLS columns, the peak-to-peak amplitude and timing of the maximum (June–July) in both IMAGESv2 simulations are in very good agreement with the FTIR results.

CC BY

Even though the role of plant growth in methanol budget is confirmed by its seasonality, large uncertainties remain on the methanol budget. Thanks to the improvement of the information content of our retrieval and therefore our vertical resolution, our partial column time series should contribute to better constraints for model simulations and therefore may lead to a better understanding of methanol budget.

Acknowledgements. The University of Liège involvement has primarily been supported by the PRODEX and SSD programs funded by the Belgian Federal Science Policy Office (Belspo), Brussels. The Swiss GAW-CH program is further acknowledged. E. Mahieu is Research Associate with the F.R.S. – FNRS. The FRS-FNRS and the Fédération Wallonie Bruxelles contributed to observational activities support. We thank the International Foundation High Altitude Research Stations Jungfraujoch and Gornergrat (HFSJG, Bern) for supporting the facilities needed to perform the observations. The contribution of BIRA-IASB was supported by the PRODEX projects A3C (2011–2013) and ACROSAT (2014–2015) funded by Belspo. The ACE mission is supported primarily by the Canadian Space Agency. We further acknowledge the vital contribution from all the Belgian colleagues in performing the Jungfraujoch observations used here.

References

Atkinson, R., Baulch, D. L., Cox, R. A., Crowley, J. N., Hampson, R. F., Hynes, R. G., Jenkin, M. E., Rossi, M. J., Troe, J., and IUPAC Subcommittee: Evaluated kinetic and photochemical data for atmospheric chemistry: Volume II – gas phase reactions of organic species, Atmos. Chem. Phys., 6, 3625–4055, doi:10.5194/acp-6-3625-2006, 2006.

Barret, B., De Mazière, M., and Demoulin, P.: Retrieval and characterization of ozone profiles from solar infrared spectra at the Jungfraujoch, J. Geophys. Res., 107, 4788, doi:10.1029/2001JD001298, 2002.

Beer, R., Shephard, M. W., Kulawik, S. S., Clough, S. A., Eldering, A., Bowman, K. W., Sander, S. P., Fisher, B. M., Payne, V. H., Luo, M., Osterman, G. B., and Worden, J. R.: First satellite observations of lower tropospheric ammonia and methanol, Geophys. Res. Lett., 35, L09801, doi:10.1029/2008GL033642, 2008.

AMTD
7, 4659–4692, 2014

Bernath, P. F., McElroy, C. T., Abrams, M. C., Boone, C. D., Butler, M., Camy-Peyret, C., Carleer, M., Clerbaux, C., Coheur, P.-F., Colin, R., DeCola, P., DeMazière, M., Drummond, J. R., Dufour, D., Evans, W. F. J., Fast, H., Fussen, D., Gilbert, K., Jennings, D. E., Llewellyn, E. J., Lowe, R. P., Mahieu, E., McConnell, J. C., McHugh, M., McLeod, S. D., Michaud, R., Midwinter, C., Nassar, R., Nichitiu, F., Nowlan, C., Rinsland, C. P., Rochon, Y. J., Rowlands, N., Semeniuk, K., Simon, P., Skelton, R., Sloan, J. J., Soucy, M.-A., Strong, K., Tremblay, P., Turnbull, D., Walker, K. A., Walkty, I., Wardle, D. A., Wehrle, V., Zander, R., and Zou, J.: Atmospheric Chemistry Experiment (ACE): mission overview, Geophys. Res. Lett., 32, L15S01, doi:10.1029/2005GL022386, 2005.

Bey, I., Jacob, D. J., Yantosca, R. M., Logan, J. A., Field, B. D., Fiore, A. M., Li, Q., Liu, H. Y., Mickley, L. J., and Schultz, M. G.: Global modeling of tropospheric chemistry with assimilated meteorology: model description and evaluation, J. Geophys. Res., 106, 23073–23095, 2001.

Boone, C. D., Walker, K. A., and Bernath, P. F.: Version 3 retrievals for the atmospheric chemistry experiment Fourier transform spectrometer (ACE-FTS), in: The Atmospheric Chemistry Experiment ACE at 10: A Solar Occultation Anthology, edited by: Bernath, P. F., Hampton, Virignia, USA, 103–127, 2013.

Cady-Pereira, K. E., Shephard, M. W., Millet, D. B., Luo, M., Wells, K. C., Xiao, Y., Payne, V. H., and Worden, J.: Methanol from TES global observations: retrieval algorithm and seasonal and spatial variability, Atmos. Chem. Phys., 12, 8189–8203, doi:10.5194/acp-12-8189-2012, 2012.

Carpenter, L. J., Lewis, A. C., Hopkins, J. R., Read, K. A., Longley, I. D., and Gallagher, M. W.: Uptake of methanol to the North Atlantic Ocean surface, Global Biogeochem. Cy., 18, GB4027, doi:10.1029/2004GB002294, 2004.

Chang, L., Palo, S., Hagan, M., Richter, J., Garcia, R., Riggin, D., and Fritts, D.: Structure of the migrating diurnal tide in the Whole Atmosphere Community Climate Model (WACCM), Adv. Space Res., 41, 1398–1407, doi:10.1016/j.asr.2007.03.035, 2008.

Drayson, S. R.: Rapid computation of the Voigt profile, J. Quant. Spectrosc. Ra., 16, 611–614, doi:10.1016/0022-4073(76)90029-7, 1976.

Duchatelet, P., Demoulin, P., Hase, F., Ruhnke, R., Feng, W., Chipperfield, M. P., Bernath, P. F., Boone, C. D., Walker, K. A., and Mahieu, E.: Hydrogen fluoride total and partial column time series above the Jungfraujoch from long-term FTIR measurements: impact of the line-shape model, characterization of the error budget and seasonal cycle, and comparison with satellite and model data, J. Geophys. Res., 115, D22306, doi:10.1029/2010JD014677, 2010.

AMTD
7, 4659–4692, 2014

Dufour, G., Boone, C. D., Rinsland, C. P., and Bernath, P. F.: First space-borne measurements of methanol inside aged southern tropical to mid-latitude biomass burning plumes using the ACE-FTS instrument, Atmos. Chem. Phys., 6, 3463–3470, doi:10.5194/acp-6-3463-2006, 2006.

Dufour, G., Szopa, S., Hauglustaine, D. A., Boone, C. D., Rinsland, C. P., and Bernath, P. F.: The influence of biogenic emissions on upper-tropospheric methanol as revealed from space, Atmos. Chem. Phys., 7, 6119–6129, doi:10.5194/acp-7-6119-2007, 2007.

Duncan, B. N., Logan, J. A., Bey, I., Megretskaia, I. A., Yantosca, R. M., Novelli, P. C., Jones, N. B., and Rinsland, C. P.: Global budget of CO, 1988–1997: source estimates and validation with a global model, J. Geophys. Res.-Atmos., 112, D22301, doi:10.1029/2007JD008459, 2007.

Fall, R.: Abundant oxygenates in the atmosphere: a biochemical perspective, Chem. Rev., 103, 4941–4952, doi:10.1021/cr0206521, 2003.

Fehsenfeld, F. C., Ancellet, G., Bates, T. S., Goldstein, A. H., Hardesty, R. M., Honrath, R., Law, K. S., Lewis, A. C., Leaitch, R., McKeen, S., Meagher, J., Parrish, D. D., Pszenny, A. A. P., Russell, P. B., Schlager, H., Seinfeld, J., Talbot, R., and Zbinden, R.: International Consortium for Atmospheric Research on Transport and Transformation (ICARTT): North America to Europe – overview of the 2004 summer field study, J. Geophys. Res., 111, D23S01, doi:10.1029/2006JD007829, 2006.

Galbally, I. E. and Kirstine, W.: The production of methanol by flowering plants and the global cycle of methanol, J. Atmos. Chem., 43, 195–229, doi:10.1023/A:1020684815474, 2002.

Gardiner, T., Forbes, A., de Mazière, M., Vigouroux, C., Mahieu, E., Demoulin, P., Velazco, V., Notholt, J., Blumenstock, T., Hase, F., Kramer, I., Sussmann, R., Stremme, W., Mellqvist, J., Strandberg, A., Ellingsen, K., and Gauss, M.: Trend analysis of greenhouse gases over Europe measured by a network of ground-based remote FTIR instruments, Atmos. Chem. Phys., 8, 6719–6727, doi:10.5194/acp-8-6719-2008, 2008.

Harrison, J. J., Allen, N. D. C., and Bernath, P. F.: Infrared absorption cross sections for methanol, J. Quant. Spectrosc. Ra., 113, 2189–2196, doi:10.1016/j.jqsrt.2012.07.021, 2012.

Hase, F., Hannigan, J. W., Coffey, M. T., Goldman, A., Höpfner, M., Jones, N. B., Rinsland, C. P., and Wood, S. W.: Intercomparison of retrieval codes used for the analysis of high-resolution, ground-based FTIR measurements, J. Quant. Spectrosc. Ra., 87, 25–52, doi:10.1016/j.jqsrt.2003.12.008, 2004.

AMTD
7, 4659–4692, 2014

Long-term evolution and seasonal modulation of methanol

W. Bader et al.

Hase, F., Demoulin, P., Sauval, A. J., Toon, G. C., Bernath, P. F., Goldman, A., Hannigan, J. W., and Rinsland, C. P.: An empirical line-by-line model for the infrared solar transmittance spectrum from 700 to 5000 cm(-1), J. Quant. Spectrosc. Ra., 102, 450–463, doi:10.1016/j.jqsrt.2006.02.026, 2006.

Heikes, B. G., Chang, W., Pilson, M. E. Q., Swift, E., Singh, H. B., Guenther, A., Jacob, D. J., Field, B. D., Fall, R., Riemer, D., and Brand, L.: Atmospheric methanol budget and ocean implication, Global Biogeochem. Cy., 16, 1133, doi:10.1029/2002GB001895, 2002.

Jacob, D. J.: Atmospheric budget of acetone, J. Geophys. Res., 107, ACH5.1–ACH5.17, doi:10.1029/2001JD000694, 2002.

Jacob, D. J., Field, B. D., Li, Q., Blake, D. R., de Gouw, J., Warneke, C., Hansel, A., Wisthaler, A., Singh, H. B., and Guenther, A.: Global budget of methanol: constraints from atmospheric observations, J. Geophys. Res., 110, D08303, doi:10.1029/2004JD005172, 2005.

Jiménez, E., Gilles, M., and Ravishankara, A.: Kinetics of the reactions of the hydroxyl radical with CH_3OH and C_2H_5OH between 235 and 360 K, J. Photoch. Photobio. A, 157, 237–245, doi:10.1016/S1010-6030(03)00073-X, 2003.

Karl, T., Guenther, A., Spirig, C., Hansel, A., and Fall, R.: Seasonal variation of biogenic VOC emissions above a mixed hardwood forest in northern Michigan, Geophys. Res. Lett., 30, 2186, doi:10.1029/2003GL018432, 2003.

Krol, M.: Can the variability in tropospheric OH be deduced from measurements of 1,1,1-trichloroethane (methyl chloroform)?, J. Geophys. Res., 108, 4125, doi:10.1029/2002JD002423, 2003.

Laffineur, Q., Aubinet, M., Schoon, N., Amelynck, C., Müller, J.-F., Dewulf, J., Van Langenhove, H., Steppe, K., and Heinesch, B.: Abiotic and biotic control of methanol exchanges in a temperate mixed forest, Atmos. Chem. Phys., 12, 577–590, doi:10.5194/acp-12-577-2012, 2012.

Legreid, G., Folini, D., Staehelin, J., Balzani Lööv, J., Steinbacher, M., and Reimann, S.: Measurements of organic trace gases including oxygenated volatile organic compounds at the high alpine site Jungfraujoch (Switzerland): seasonal variation and source allocations, J. Geophys. Res., 113, D05307, doi:10.1029/2007JD008653, 2008.

Logan, J. A., Prather, M. J., Wofsy, S. C., and McElroy, M. B.: Tropospheric chemistry: a global perspective, J. Geophys. Res., 86, 7210, doi:10.1029/JC086iC08p07210, 1981.

Madronich, S. and Calvert, J. G.: Permutation reactions of organic peroxy radicals in the troposphere, J. Geophys. Res., 95, 5697–5715, doi:10.1029/JD095iD05p05697, 1990.

CC BY

Millet, D. B., Jacob, D. J., Turquety, S., Hudman, R. C., Wu, S., Fried, A., Walega, J., Heikes, B. G., Blake, D. R., Singh, H. B., Anderson, B. E., and Clarke, A. D.: Formaldehyde distribution over North America: implications for satellite retrievals of formaldehyde columns and isoprene emission, J. Geophys. Res., 111, D24S02, doi:10.1029/2005JD006853, 2006.

Millet, D. B., Jacob, D. J., Custer, T. G., de Gouw, J. A., Goldstein, A. H., Karl, T., Singh, H. B., Sive, B. C., Talbot, R. W., Warneke, C., and Williams, J.: New constraints on terrestrial and oceanic sources of atmospheric methanol, Atmos. Chem. Phys., 8, 6887–6905, doi:10.5194/acp-8-6887-2008, 2008.

Paton-Walsh, C., Wilson, S. R., Jones, N. B., and Griffith, D. W. T.: Measurement of methanol emissions from Australian wildfires by ground-based solar Fourier transform spectroscopy, Geophys. Res. Lett., 35, L08810, doi:10.1029/2007GL032951, 2008.

Razavi, A., Karagulian, F., Clarisse, L., Hurtmans, D., Coheur, P. F., Clerbaux, C., Müller, J. F., and Stavrakou, T.: Global distributions of methanol and formic acid retrieved for the first time from the IASI/MetOp thermal infrared sounder, Atmos. Chem. Phys., 11, 857–872, doi:10.5194/acp-11-857-2011, 2011.

Rinsland, C. P., Jones, N. B., Connor, B. J., Logan, J. A., Pougatchev, N. S., Goldman, A., Murcray, F. J., Stephen, T. M., Pine, A. S., Zander, R., Mahieu, E., and Demoulin, P.: Northern and Southern Hemisphere ground-based infrared spectroscopic measurements of tropospheric carbon monoxide and ethane, J. Geophys. Res., 103, 28197–28217, doi:10.1029/98JD02515, 1998.

Rinsland, C. P., Mahieu, E., Chiou, L., and Herbin, H.: First ground-based infrared solar absorption measurements of free tropospheric methanol (CH3OH): multidecade infrared time series from Kitt Peak (31.9° N 111.6° W): trend, seasonal cycle, and comparison with previous measurements, J. Geophys. Res., 114, D04309, doi:10.1029/2008JD011003, 2009.

Rodgers, C. D.: Characterization and error analysis of profiles retrieved from remote sounding measurements, J. Geophys. Res., 95, 5587–5595, doi:10.1029/JD095iD05p05587, 1990.

Rodgers, C.: Inverse Methods For Atmospheric Sounding, Vol. 2 of Series on Atmospheric, Oceanic and Planetary Physics, 2000.

Rothman, L. S., Jacquemart, D., Barbe, A., Chris Benner, D., Birk, M., Brown, L. R., Carleer, M. R., Chackerian, C., Chance, K., Coudert, L. H., Dana, V., Devi, V. M., Flaud, J.-M., Gamache, R. R., Goldman, A., Hartmann, J.-M., Jucks, K. W., Maki, A. G., Mandin, J.-Y., Massie, S. T., Orphal, J., Perrin, A., Rinsland, C. P., Smith, M. A. H., Tennyson, J., Tolchenov, R. N., Toth, R. A., Vander Auwera, J., Varanasi, P., and Wagner, G.: The HI-

CC BY

TRAN 2004 molecular spectroscopic database, J. Quant. Spectrosc. Ra., 96, 139–204, doi:10.1016/j.jqsrt.2004.10.008, 2005.

Rothman, L. S., Gordon, I. E., Barbe, A., Benner, D. C., Bernath, P. F., Birk, M., Boudon, V., Brown, L. R., Campargue, A., Champion, J.-P., Chance, K., Coudert, L. H., Dana, V., Devi, V. M., Fally, S., Flaud, J.-M., Gamache, R. R., Goldman, A., Jacquemart, D., Kleiner, I., Lacome, N., Lafferty, W. J., Mandin, J.-Y., Massie, S. T., Mikhailenko, S. N., Miller, C. E., Moazzen-Ahmadi, N., Naumenko, O. V., Nikitin, A. V., Orphal, J., Perevalov, V. I., Perrin, A., Predoi-Cross, A., Rinsland, C. P., Rotger, M., Šimečková, M., Smith, M. A. H., Sung, K., Tashkun, S. A., Tennyson, J., Toth, R. A., Vandaele, A. C., and Vander Auwera, J.: The HITRAN 2008 molecular spectroscopic database, J. Quant. Spectrosc. Ra., 110, 533–572, doi:10.1016/j.jqsrt.2009.02.013, 2009.

Schade, G. W. and Goldstein, A. H.: Fluxes of oxygenated volatile organic compounds from a ponderosa pine plantation, J. Geophys. Res., 106, 3111–3123, doi:10.1029/2000JD900592, 2001.

Schade, G. W. and Goldstein, A. H.: Seasonal measurements of acetone and methanol: abundances and implications for atmospheric budgets, Global Biogeochem. Cy., 20, GB1011, doi:10.1029/2005GB002566, 2006.

Singh, H. B., O'Hara, D., Herlth, D., Sachse, W., Blake, D. R., Bradshaw, J. D., Kanakidou, M., and Crutzen, P. J.: Acetone in the atmosphere: distribution, sources, and sinks, J. Geophys. Res., 99, 1805–1819, doi:10.1029/93JD00764, 1994.

Singh, H., Chen, Y., Staudt, A., Jacob, D., Blake, D., Heikes, B., and Snow, J.: Evidence from the Pacific troposphere for large global sources of oxygenated organic compounds, Nature, 410, 1078–1081, doi:10.1038/35074067, 2001.

Singh, H. B., Brune, W. H., Crawford, J. H., Jacob, D. J., and Russell, P. B.: Overview of the summer 2004 Intercontinental Chemical Transport Experiment–North America (INTEX-A), J. Geophys. Res.-Atmos., 111, D24S01, doi:10.1029/2006JD007905, 2006.

Stavrakou, T., Guenther, A., Razavi, A., Clarisse, L., Clerbaux, C., Coheur, P.-F., Hurtmans, D., Karagulian, F., De Mazière, M., Vigouroux, C., Amelynck, C., Schoon, N., Laffineur, Q., Heinesch, B., Aubinet, M., Rinsland, C., and Müller, J.-F.: First space-based derivation of the global atmospheric methanol emission fluxes, Atmos. Chem. Phys., 11, 4873–4898, doi:10.5194/acp-11-4873-2011, 2011.

Tie, X., Guenther, A., and Holland, E.: Biogenic methanol and its impacts on tropospheric oxidants, Geophys. Res. Lett., 30, 1881, doi:10.1029/2003GL017167, 2003.

CC BY

Tyndall, G. S., Cox, R. A., Granier, C., Lesclaux, R., Moortgat, G. K., Pilling, M. J., Ravishankara, A. R., and Wallington, T. J.: Atmospheric chemistry of small organic peroxy radicals, J. Geophys. Res., 106, 12157–12182, doi:10.1029/2000JD900746, 2001.

Vigouroux, C., De Mazière, M., Demoulin, P., Servais, C., Hase, F., Blumenstock, T., Kramer, I., Schneider, M., Mellqvist, J., Strandberg, A., Velazco, V., Notholt, J., Sussmann, R., Stremme, W., Rockmann, A., Gardiner, T., Coleman, M., and Woods, P.: Evaluation of tropospheric and stratospheric ozone trends over Western Europe from ground-based FTIR network observations, Atmos. Chem. Phys., 8, 6865–6886, doi:10.5194/acp-8-6865-2008, 2008.

Vigouroux, C., Stavrakou, T., Whaley, C., Dils, B., Duflot, V., Hermans, C., Kumps, N., Metzger, J.-M., Scolas, F., Vanhaelewyn, G., Müller, J.-F., Jones, D. B. A., Li, Q., and De Mazière, M.: FTIR time-series of biomass burning products (HCN, C_2H_6, C_2H_2, CH_3OH, and HCOOH) at Reunion Island (21° S, 55° E) and comparisons with model data, Atmos. Chem. Phys., 12, 10367–10385, doi:10.5194/acp-12-10367-2012, 2012.

von Kuhlmann, R., Lawrence, M. G., Crutzen, P. J., and Rasch, P. J.: A model for studies of tropospheric ozone and nonmethane hydrocarbons: model description and ozone results, J. Geophys. Res., 108, 4294, doi:10.1029/2002JD002893, 2003a.

von Kuhlmann, R., Lawrence, M. G., Crutzen, P. J., and Rasch, P. J.: A model for studies of tropospheric ozone and nonmethane hydrocarbons: model evaluation of ozone-related species, J. Geophys. Res., 108, 4729, doi:10.1029/2002JD003348, 2003b.

Warneke, C., Karl, T., Judmaier, H., Hansel, A., Jordan, A., Lindinger, W., and Crutzen, P. J.: Acetone, methanol, and other partially oxidized volatile organic emissions from dead plant matter by abiological processes: significance for atmospheric HO_x chemistry, Global Biogeochem. Cy., 13, 9–17, doi:10.1029/98GB02428, 1999.

Warneke, C., de Gouw, J. A., Goldan, P. D., Kuster, W. C., Williams, E. J., Lerner, B. M., Jakoubek, R., Brown, S. S., Stark, H., Aldener, M., Ravishankara, A. R., Roberts, J. M., Marchewka, M., Bertman, S., Sueper, D. T., McKeen, S. A., Meagher, J. F., and Fehsenfeld, F. C.: Comparison of daytime and nighttime oxidation of biogenic and anthropogenic VOCs along the New England coast in summer during New England Air Quality Study 2002, J. Geophys. Res., 109, D10309, doi:10.1029/2003JD004424, 2004.

Wells, K. C., Millet, D. B., Hu, L., Cady-Pereira, K. E., Xiao, Y., Shephard, M. W., Clerbaux, C. L., Clarisse, L., Coheur, P.-F., Apel, E. C., de Gouw, J., Warneke, C., Singh, H. B., Goldstein, A. H., and Sive, B. C.: Tropospheric methanol observations from space: retrieval eval-

AMTD
7, 4659–4692, 2014

CC BY

uation and constraints on the seasonality of biogenic emissions, Atmos. Chem. Phys., 12, 5897–5912, doi:10.5194/acp-12-5897-2012, 2012.
Xu, L.-H., Lees, R. M., Wang, P., Brown, L. R., Kleiner, I., and Johns, J. W. C.: New assignments, line intensities, and HITRAN database for CH_3OH at 10 µm, J. Mol. Spectrosc., 228, 453–470, doi:10.1016/j.jms.2004.05.017, 2004.
Zander, R., Mahieu, E., Demoulin, P., Duchatelet, P., Roland, G., Servais, C., Mazière, M. D., Reimann, S., and Rinsland, C. P.: Our changing atmosphere: evidence based on long-term infrared solar observations at the Jungfraujoch since 1950, Sci. Total Environ., 391, 184–195, doi:10.1016/j.scitotenv.2007.10.018, 2008.

Discussion Paper | Discussion Paper | Discussion Paper | Discussion Paper |

Table 1. Error budget for total and all three partial columns. TC: total column, Tropo: tropospheric column, LT: lower tropospheric layer, UTLS: upper troposphere/lower stratosphere.

Error Sources	Max. Error (%)				
	TC	Tropo	LT	UTLS	Comments
Variability	46	50	57	48	
Systematic Errors (%)					
	TC	Tropo	LT	UTLS	
Line intensity CH_3OH	7.02	7.11	6.39	9.22	Xu et al. (2004)
Line Intensity interfering gases	1.00	1.73	3.96	0.91	Rothman et al. (2009)
ILS	0.41	0.33	1.19	2.39	±10% misalignment
Forward model	1	< 1	< 1	< 1	Retrieval algorithm-related
Total	7.17	7.39	7.68	9.62	
Random Errors (%)					
	TC	Tropo	LT	UTLS	
P-T profiles	1.2	2.3	11.3	8.6	From NCEP
SZA	0.2	0.4	3.1	1.4	0.2°
Smoothing	0.4	4.4	16.1	15.2	Barret et al. (2002)
Measurement noise	5.2	19.4	35.9	37.5	
Model parameters	0.7	0.6	0.5	1.2	
Total	5.37	20.04	40.18	41.43	
Relative Standard Deviation	6.60	8.34	22.59	21.11	

AMTD
7, 4659–4692, 2014

cc BY

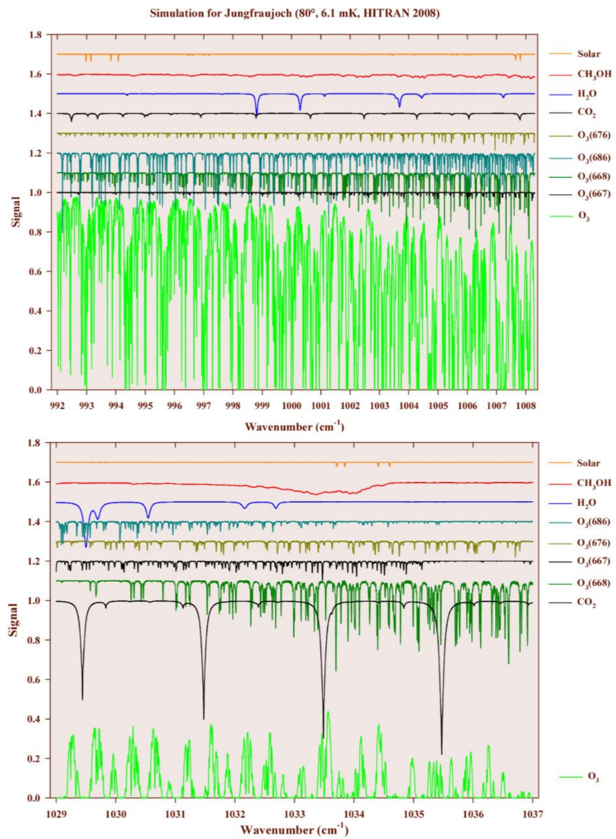

Fig. 1. Simulation for Jungfraujoch, 80° zenith angle, 6.1 mK. For both windows, we display the synthetic spectra for individual contributors (see color codes). HITRAN 2008 and averaged mixing ratio profiles based on the WACCM model climatology have been used for the simulations, except for CH_3OH for which our a priori was used (see text). For clarity, the contributions of each species have been vertically shifted.

AMTD
7, 4659–4692, 2014

CC BY

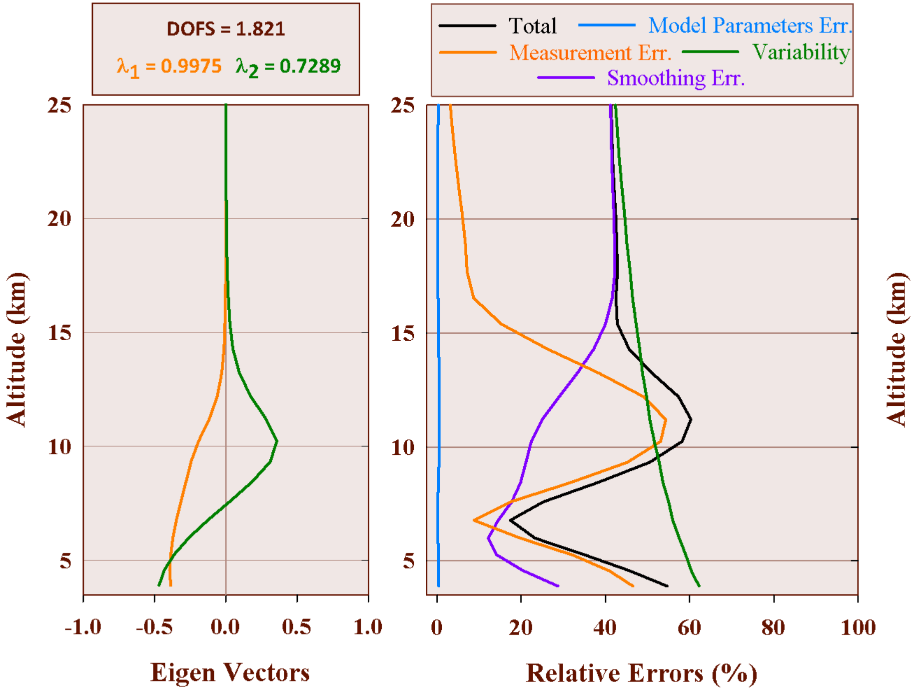

Fig. 2. Typical results for information content and error budget. Left frame: first eigen vectors and corresponding eigenvalues. Right frame: error budget, with identification of the main error components, together with the assumed variability (see color codes and Table 1 for additional information).

AMTD
7, 4659–4692, 2014

CC BY

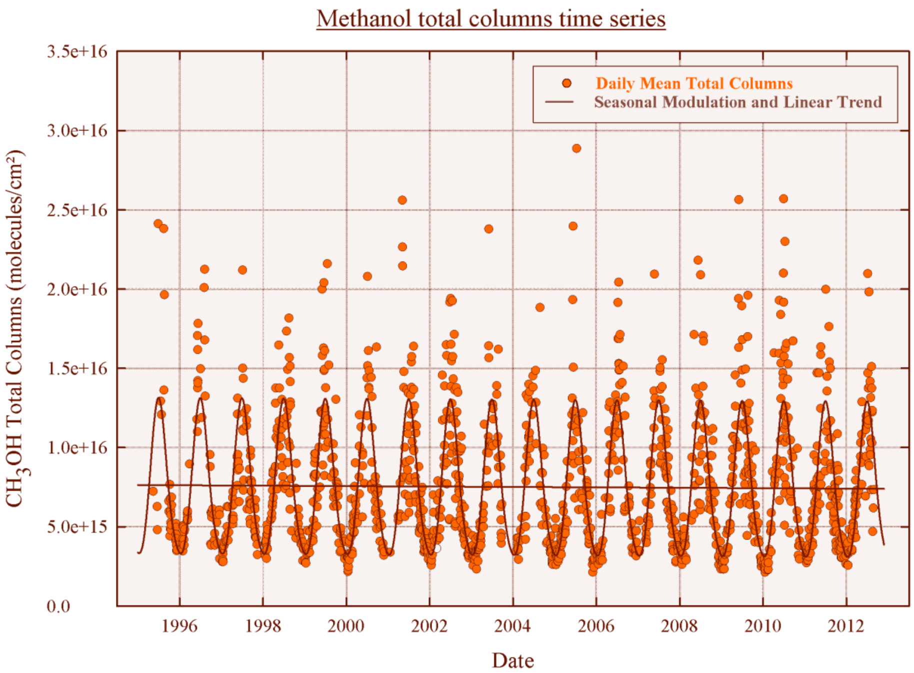

Fig. 3. Daily mean total (orange circles) column time series of CH_3OH above Jungfraujoch. Brown curves show the linear and seasonal trend components computed with the bootstrap resampling method (Gardiner et al., 2008).

AMTD
7, 4659–4692, 2014

Long-term evolution and seasonal modulation of methanol

W. Bader et al.

CC BY

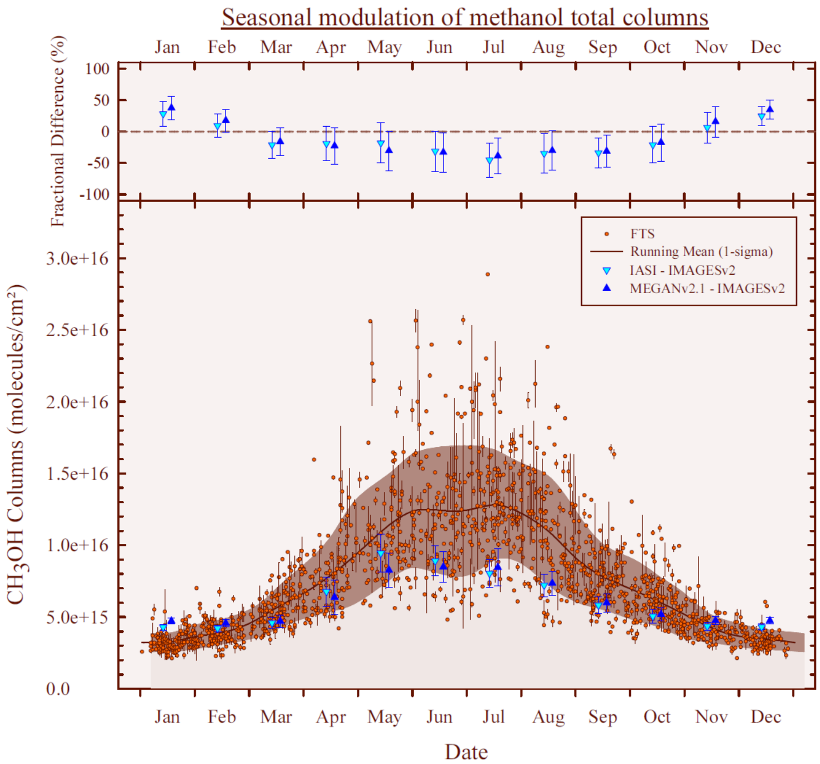

Fig. 4. Seasonal modulation of methanol total columns. Dots with vertical lines represent the daily mean total columns over a 1 year time base and their associated standard deviation. The brown curve corresponds to a running mean fit to all data points, with a 15 day step and a 2 month wide integration time. The area corresponds to the 1-σ standard deviation associated to the running mean curve. Up and down blue triangles are monthly means of the model IMAGESv2 simulations for MEGAN and IASI respectively. Upper frame shows monthly fractional difference between FTIR results and IMAGESv2 simulations.

AMTD
7, 4659–4692, 2014

CC BY

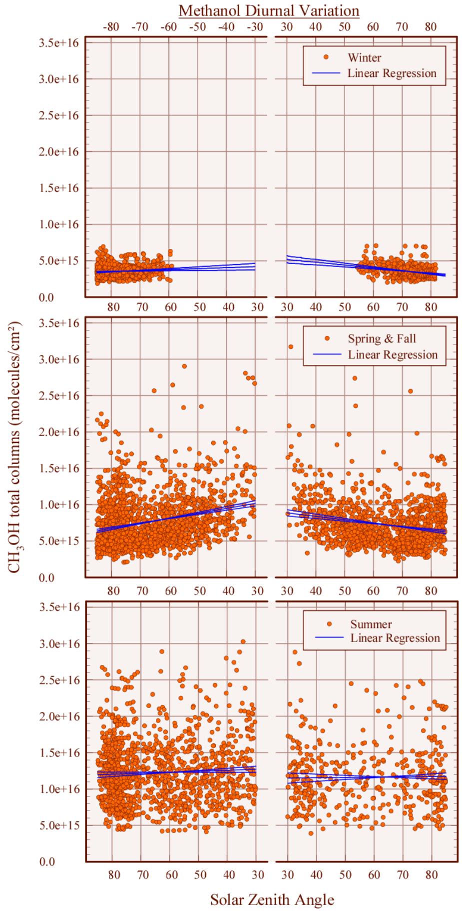

Fig. 5. Methanol diurnal variation. Total columns vs. the solar zenith angle for winter, summer and the rest of the year. Blue lines represent linear regressions.

CC BY

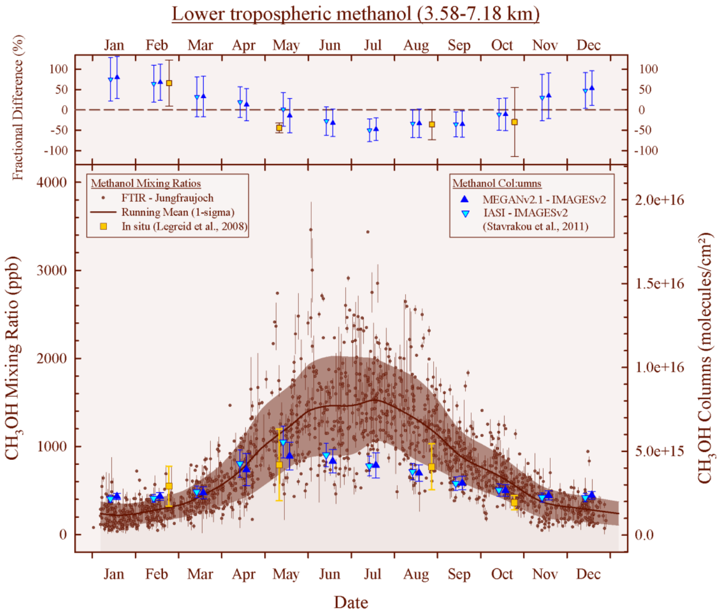

Fig. 6. Lower-tropospheric methanol (3.58–7.18 km). Dots with vertical lines represent the daily mean lower-tropospheric columns over a 1 year time base and their associated standard deviation. The brown curve corresponds to a running mean fit to all data points, with a 15 day step and a 2 month wide integration time. The area corresponds to the 1-σ standard deviation associated to the running mean curve. Up and down blue triangles are monthly means of the model IMAGESv2 simulations for MEGAN and IASI respectively (Stavrakou et al., 2011). Yellow squares are seasonal means of methanol in situ measurements (Legreid et al., 2008). The upper panel shows monthly fractional difference between FTIR results and IMAGESv2 simulations and seasonal fraction difference with in situ measurements.

AMTD

7, 4659–4692, 2014

CC BY

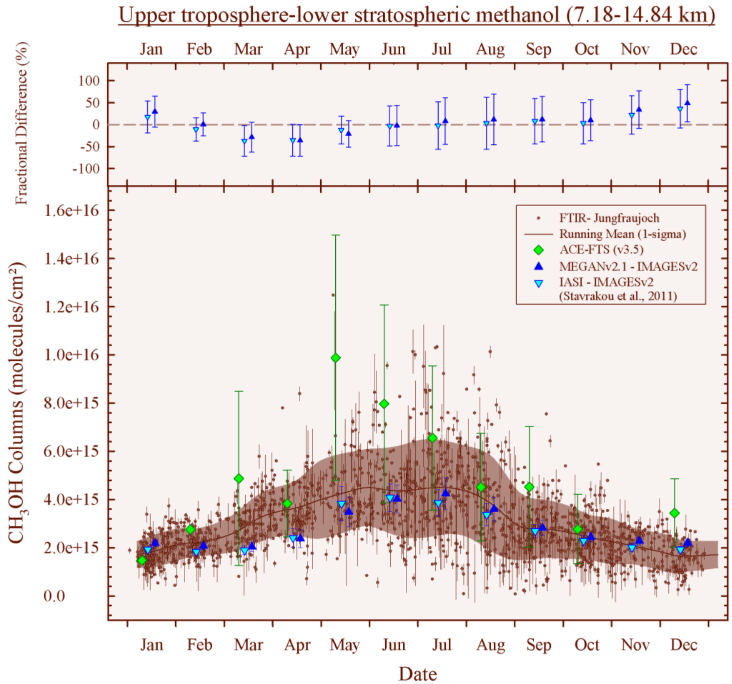

Fig. 7. Upper troposphere-lower stratospheric methanol (7.18–14.84 km). Dots with vertical lines representing daily mean lower-tropospheric columns over a 1 year time base and their associated standard deviation. The brown curve corresponds to a running mean fit to all data points, with a 15 day step and a 2 month wide integration time. The area corresponds to the 1-σ standard deviation associated to the running mean curve. Up and down blue triangles are monthly means of the model IMAGESv2 simulations for MEGAN and IASI respectively (Stavrakou et al., 2011). Green diamonds are monthly means of methanol retrieved from ACE-FTS occultations with the error bars representing the standard deviation (2-σ). Upper frame show monthly fractional difference between FTIR results and IMAGESv2 simulations and ACE-FTS results.

AMTD
7, 4659–4692, 2014

CC BY